UNIVERSITÀ DEGLI STUDI
DI TRENTO

Department of Industrial Engineering

Reviewer #1:

Q1. The interactions between the rGO and E-glass fiber should be clarified since it play a crucial role in affecting the interfacial quality between the fiber and the epoxy matrix.

Response: A detailed study of the interaction between a coating of GO electrophoretically deposited onto E-glass and subsequently reduced into rGO by exposure to hydrazine hydrate at 100°C fiber has been recently performed. The obtained results have been summarized in a manuscript [1] recently submitted for publication in *Composites Part B: Engineering.* Spectroscopic techniques like Fourier transform infrared, Raman spectroscopy, X-ray photoelectron spectroscopy and X-ray diffraction showed that the treatment with hydrazine replaces oxygen functional groups and also induces roughness, a structural disorder as well as decreases the interlayer separation in the transition from graphene oxide (GO) to reduced graphene oxide (rGO). Treatment with hydrazine reduces adhesion and friction force against diamond like carbon coated Si probe (DLC AFM) at the basal plain of the coatings. Investigation at the edges revealed that the presence of oxygen functional group leads to higher shear strength with glass-fiber which reduces after treatment with hydrazine.

In particular, the following interfacial shear strength values have been measured and reported in the submitted manuscript:

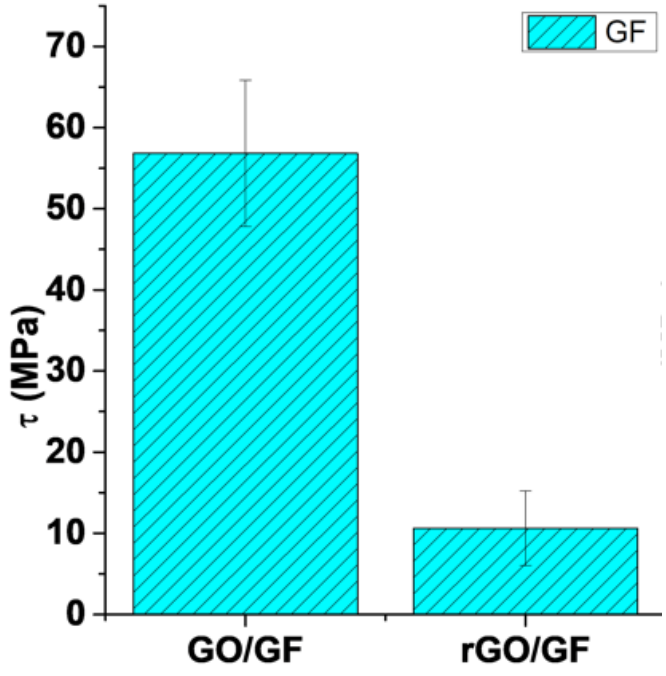

The above considerations have been added in the revised version of this manuscript.

Via Sommarive 9 – 38123 Trento, Italy - Tel. +39 0461/282500-2503 , Fax +39 0461281977

Q2. Figure 5: the presence of GO and rGO coating on the fiber surface showed different: the GO sheets cannot wrap the fiber, while the rGO coating seems to well wrap around the fiber. Is the content of GO and rGO on the fiber same?

Response: We thank the referee for pointing out this issue. In fact this conclusions comes from the fact that the selected SEM picture is not representing the situation commonly encountered for the GO coated fibers. In fact, GO coating generally appeared to be homogenous on the fibers. Therefore, Figure 5b is replaced with the following more representative picture.

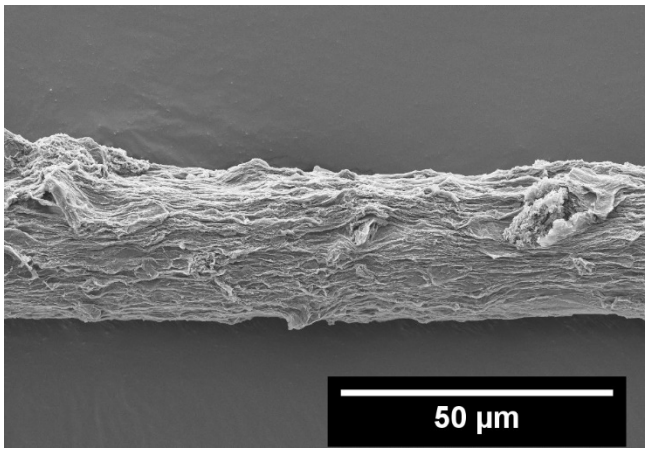

Q3. The thickness of rGO layer on the fiber should be very important on influencing the mechanical and electrical properties of the final composites. The authors are encouraged to optimize the content of rGO on the fiber.

Response: This aspect has been investigated in previous publications by this research group. In particular, as reported in Figure 4 of our prior publication [2] a relationship has been established between the voltage applied during the electrophorectic deposition (EPD) process and the amount (weight) of GO coated onto the glass fibers:

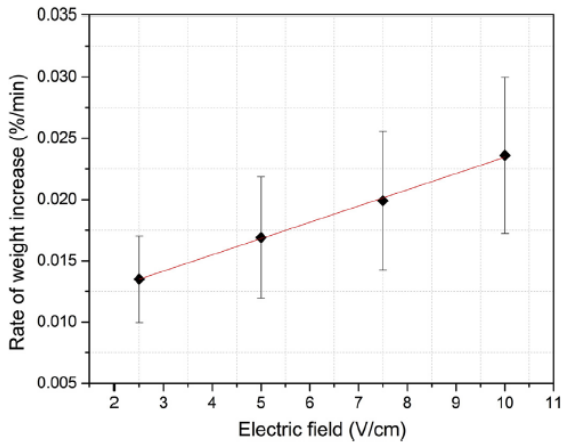

Fig. 4. Rate of weight increase of GO coated glass fiber as a function of the applied field during EPD process.

On the other hand, it has been also proved [3] that as the applied EPD voltage increases, the resulting interfacial shear strength (ISS) also increases.

37th Risø International Symposium on Materials Science IOP Publishing
IOP Conf. Series: Materials Science and Engineering **139** (2016) 012004 doi:10.1088/1757-899X/139/1/012004

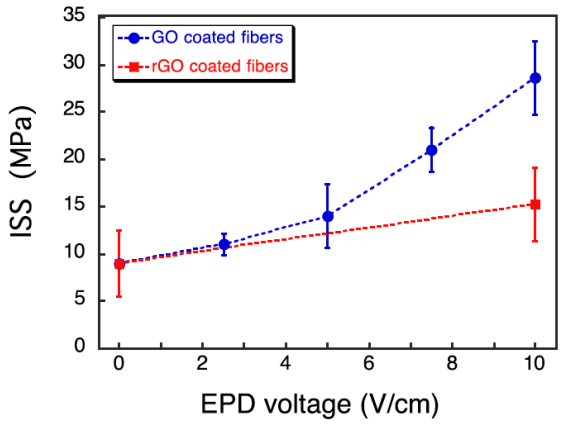

Figure 10. ISS values as determined by the fragmentation test performed on microcomposites containing GF_2 fiber coated with GO or rGO applied by electrophoretic deposition (EPD) under various applied voltages.

In the present manuscript, the EPD conditions (and therefore the rGO content on the fibers) have been selected in order to maximize the ISS values. These considerations have been briefly reported in the revised manuscript.

Q4. After chemical reduction, was the GO completely reduced? On the other hand, did the hydrazine hydrate vapors affect the property and structure of fiber during the reduction process?

Response: The XPS data reported in Table 3 of the manuscript indicate that the oxygen and carbon percentage in GO and rGO are of 34.2% and 9.9%, respectively. This clearly indicates that the chemical reduction process was not able to completely reduce GO.

Q5. From Figure 5c, some micro-cracks can be observed in rGO layer. The interaction among the rGO layer on the fiber should be illustrated to clarify the improved interlaminar shear strength when compared to bare fiber.

Response: The micro-cracks that can be observed in the rGO coating are the result of the selected deposition method. Friction force atomic force microscopy tests described in [1, 2] evidenced that a good interfacial adhesion exist between both GO coating and the glass fibers. The chemical reduction process leads to a reduction of such adhesion level (see response to Q1).

Q6. The GO coating produced higher improvements in mechanical properties than the rGO coating. The related failure mechanisms should be discussed based on the micro-structure analysis.

Response: We agree with the referee suggestion. Therefore, we propose to add additional information on the morphology of the fracture surfaces of post-mortem DCB fracture toughness specimens (new Figure 11 in the revised manuscript).

Figure 11.

a) 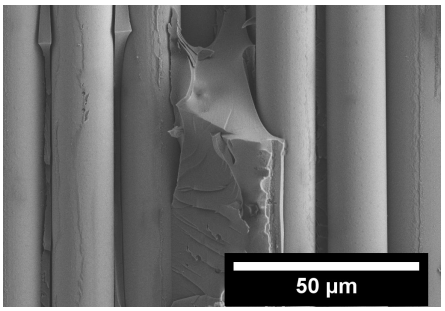

b) 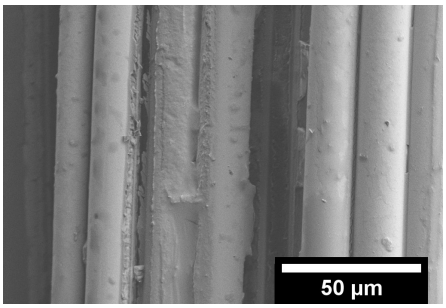

c) 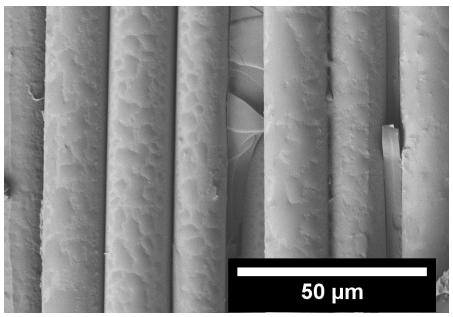

Interesting observations were obtained during the analysis of the fracture surfaces obtained after mode I fracture toughness test of DCB specimens. The fracture surfaces of Ep-GF composite (Figure 11a) indicate a weak fiber-matrix interaction revealed by the presence of the glass fibers with a clean surface. On the other hand, the fracture surfaces of Ep-GO-GF (Figure 11b) shows a number of fibers coated with the remnants of epoxy matrix which could be associated to a good interfacial adhesion. It can be visualized from the FESEM images that the fibers are bonded together with continuous epoxy resin hence suggesting the influence of GO coating on fibers promoting strong inter-fiber interactions due to epoxy/GO/GF system. At the end, the fracture surfaces obtained from the Ep-rGO-GF composite system gives a different picture in which the fiber surfaces are covered totally with a continuous coating (Figure 11c). A detail examination reveals that the rGO coating had a different morphology as compared to the epoxy matrix. The lower values of NL during mode I fracture toughness is a clear evidence that debonding took place at the epoxy/rGO interface. This is correlated to the fact that rGO sheets, due to unavailability of the oxygen based functional groups, offered a weaker interfacial adhesion towards the epoxy matrix.

Q7. Figure 14: the resistance change title of Figures 4b and 4d are not shown. The title of Figure 15 is missing. Figure 15 should be Figure 16; and Figure 16 should be Figure 17.

Response: Corrections have been performed in the revised version of the manuscript to avoid this issue.

Q8. Page 26: Figure 15 was not discussed in the text. The authors should check this. Moreover, the different resistance changes with the strain should be explained.

Response: Figure 15 has been removed in the revised of the manuscript since we realized that it does not convey additional information and in order to limit the number of figures.

References

[1] Tripathi M, Mahmood H, Novel D, Iacob E, Vanzetti L, Bartali R, et al. Nanoscale friction of graphene oxide over glass-fibre and polystyrene Composites Part B: Engineering. submitted.
[2] Mahmood H, Tripathi M, Pugno N, Pegoretti A. Enhancement of interfacial adhesion in glass fiber/epoxy composites by electrophoretic deposition of graphene oxide on glass fibers. Compos Sci Technol. 2016;126:149-57.
[3] Pegoretti A, Mahmood H, Pedrazzoli D, Kalaitzidou K. Improving fiber/matrix interfacial strength through graphene and graphene-oxide nano platelets. IOP Conference Series: Materials Science and Engineering. 2016;139:1-12.

UNIVERSITÀ DEGLI STUDI
DI TRENTO

Department of Industrial Engineering

Reviewer #2:

Q1. What is the main form of interaction between graphene and glass fiber? Covalent or non-covalent bonding? Why?

Response: The question raised by the reviewer is actually a very important one. Unfortunately, to the best of author's knowledge the experimental distinction of covalent or non-covalent bonds at the interfaces is not simple and still represent an open issue for the interfacial studies in composite materials. For as the present case is concerned, we can certainly claim that there are no clear reasons why covalent bonds should form between the deposited graphene oxide (GO) layers and the glass fiber surface. Therefore, the most probable case is the presence of non-covalent bonds between the oxygen functional groups of GO and the (unknown) groups of the fiber sizing.

Q2. The sub-section "3.2 Fiber-matrix adhesion in single-fiber model composites" could be strengthened by the analysis of the interfacial interaction as requested above.

Response: A detailed study of the interaction between a coating of GO electrophoretically deposited onto E-glass and subsequently reduced into rGO by exposure to hydrazine hydrate at 100°C fiber has been recently performed. The obtained results have been summarized in a manuscript [1] recently submitted for publication in *Composites Part B: Engineering.* Spectroscopic techniques like Fourier transform infrared, Raman spectroscopy, X-ray photoelectron spectroscopy and X-ray diffraction showed that the treatment with hydrazine replaces oxygen functional groups and also induces roughness, a structural disorder as well as decreases the interlayer separation in the transition from graphene oxide (GO) to reduced graphene oxide (rGO). Treatment with hydrazine reduces adhesion and friction force against diamond like carbon coated Si probe (DLC AFM) at the basal plain of the coatings. Investigation at the edges revealed that the presence of oxygen functional group leads to higher shear strength with glass-fiber which reduces after treatment with hydrazine.

In particular, the following interfacial shear strength values have been measured and reported in the submitted manuscript:

Via Sommarive 9 – 38123 Trento, Italy - Tel. +39 0461/282500-2503 , Fax +39 0461281977

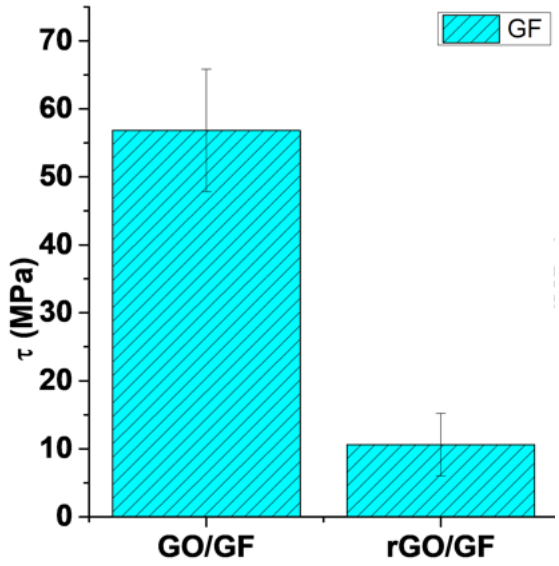

The above considerations have been added in the revised version of this manuscript.

Q3. Pages 2~3, "Coating the fibers with graphene oxide nanosheets to create an interphase in polymer matrix has been recently proven to be a successful approach to enhance the load transfer at the fiber matrix interface [22, 23]. However, the efficiency of this method has been so far explored only on model single-fiber composites." It is not true. The following papers dealt with graphene coated fabric composites possessing piezoresistive response, and should be discussed in the revised manuscript to show your grasp of the achievements in the field. M. A. Ali, et al., COMPOSITES SCIENCE AND TECHNOLOGY, 148, 2017, 106. R. Moriche, et al., COMPOSITES SCIENCE AND TECHNOLOGY, 146, 2017, 59.

Response: We thank the reviewer for the useful suggestions. The indicated references have been added along with a comment on the significance of the present work compared to the existing ones.

Q4. Why the electrodes are perpendicular to the fibers alignment (refer to Figs. 13 and 14)?

Response: The “terminals” of the resistivity measurement systems were placed perpendicular in order to measure the resistivity changes along the fiber direction thus monitoring the fiber strain during the test.

Q5. Why the low Tg epoxy, rather than high Tg epoxy, is used as the matrix?

Response: In this work, and also in that previously published in Composites Science and Technology [2], the single fiber fragmentation test has been used to quantify the interfacial shear strength of both coated and uncoated fibers to the epoxy resin. The execution of the single fiber fragmentation test requires a matrix with an elongation at break of at least three times the elongation at break of the fibers. Therefore, the selection of a low Tg epoxy matrix was need in order to satisfy this experimental requirement.

Q6. The improvement of mechanical properties including fracture toughness, ISS and ILSS should be compared with other glass fiber composites with different interfacial treatments. In-depth discussion of the underlying mechanisms should be added accordingly.

Response: A new Table 6 has been added to the manuscript to compare the system proposed in the present manuscript to the data available in the literature on composites with different interfacial treatments based on the use of graphene or graphene oxide.

References

[1] Tripathi M, Mahmood H, Novel D, Iacob E, Vanzetti L, Bartali R, et al. Nanoscale friction of graphene oxide over glass-fibre and polystyrene Composites Part B: Engineering. submitted.

[2] Mahmood H, Tripathi M, Pugno N, Pegoretti A. Enhancement of interfacial adhesion in glass fiber/epoxy composites by electrophoretic deposition of graphene oxide on glass fibers. Compos Sci Technol. 2016;126:149-57.

Mechanical properties and strain monitoring of glass-epoxy composites with graphene-coated fibers

Haroon Mahmood[1], Lia Vanzetti[2], Massimo Bersani[2], and Alessandro Pegoretti[1]*

[1] Department of Industrial Engineering, University of Trento, via Sommarive 9, 38123 Trento, Italy.

[2] Centre for Materials and Microsystems, Fondazione Bruno Kessler, via Sommarive 18, 38123 Trento, Italy.

Abstract

An engineered interphase can improve the mechanical properties of epoxy/glass composites simultaneously inducing a piezoresistive response. To prove this concept, E-glass fibers were coated with graphene oxide (GO) by electrophoretic deposition, while reduced graphene oxide (rGO) coated fibers were obtained by subsequent chemical reduction. The fiber-matrix interfacial shear strength measured by the single-fiber fragmentation test increased for both GO and rGO coated fibers. Unidirectional composites with a high content of both uncoated and coated fibers were produced and mechanically tested under various configurations (three-point bending, short beam shear and mode-I fracture toughness, creep). Composites with coated fibers performed similarly or better than composites prepared with uncoated fibers. Finally, composites with rGO coated fibers were tested for their piezoresistive response under both static and dynamic conditions. The electrical resistance changed proportionally to applied strain thus confirming the possibility of using composites with rGO coated fibers as strain sensors in load-bearing components.

Keywords: A. Glass fibres; B. Fibre/matrix bond; B. Fragmentation; B. Mechanical properties.

* corresponding author: alessandro.pegoretti@unitn.it, tel +39-0461-282452, fax +39-0461-281977

1 Introduction

The use of polymer composites for structural and non-structural applications is rapidly expanding mainly due to their high strength-to-weight ratio and corrosion resistance. The utmost requirement in a structural composite is an high level of mechanical properties which in turn largely depends on the fiber/matrix interfacial adhesion [1]. This dependence comes from the fact that an effective load transfer from matrix to the fibers is required to exploit the superior elastic and ultimate mechanical properties of high-performance fibers. This could be assured by mechanisms such as mechanical interlocking, chemical bonding or physical adhesion at the fiber/matrix interface [2]. The poor wettability of matrix or the absence of functional groups on fiber may result in an unsatisfactory load transfer process. Both academia and industry are constantly investigating new ways to design better fiber/matrix interphases in structural composites in order to assure an optimal load transfer and possibly adding new functionalities [3].

The use of nanomaterials in polymer composites and the novel properties offered by such nanocomposites have been widely investigated in recent years. The presence of nanomaterials like clays, carbon nanotubes and graphene have been proven to largely affect the properties of both thermoplastic and thermosetting matrices [4]. Especially, the advantage of using carbonaceous nanomaterials as functional filler in polymer composites has been vastly proven due to their elevated mechanical properties and high electrical conductivity [5]. This last feature led to the possibility of self-sensing or in-situ structural health monitoring of carbon nanomaterial reinforced polymer composites like in case of CNT [6-8] and graphene [9, 10]. Graphene, since its discovery in 2004, has been investigated at an exponential level in recent years due to its exceptional mechanical, electrical, optical and thermal properties [11-14]. The use of graphene in polymer composites has shown to play remarkable synergistic effects for multiple applications [15]. However, in order to obtain maximum benefit from the nanoparticles, it is necessary to reach an optimal dispersion in polymer matrices which is often quite difficult due to high surface energy of nanoparticles which results in their agglomeration [16, 17].

In case of fiber reinforced polymer composites, various studies have been conducted to prove the impact of nanoparticles in enhancing various mechanical properties [18-21]. In most of the research work reported in the open scientific literature, nanoparticles were more or less homogeneously dispersed in polymer matrices in various concentrations. Another possible approach consists in depositing nanofillers on the fiber surface thus allowing a selective modification of the interphase [3] . Coating the fibers with graphene oxide nanosheets to create an interphase in polymer matrix has been recently proven to be a successful approach to enhance the load transfer at the fiber

matrix interface [22, 23]. Graphene coated fibers have been recently utilized for strain monitoring applications in which the coating of graphene was performed by soaking (in GO solution) [24] or dip coating process (in GNP solution) [25]. However, the use of a controlled electrophoretic deposition process to create a fairly uniform and continuous graphene coating on fibers has not yet been utilized.

Hence in this paper, we explore the creation of an interphase of GO and rGO by electrophoretic deposition on glass fibers (GF) and their usage to produce fiber reinforced polymer composites with an epoxy matrix. The interfacial properties of single fiber composites with both interphases are presented and compared in this paper along with mechanical properties of high fiber volume fraction composites. For conductive composites with rGO coated fibers, the strain-monitoring/self-sensing behavior of glass fiber/epoxy composites was also investigated in detail where the change of absolute resistance due to change in strain in composites was also monitored and analyzed.

2 Experimental

2.1 Materials

All chemicals were of analytical grade and used without additional purification. Graphite powder, potassium permanganate, sulfuric acid, sodium nitrate and hydrogen peroxide were purchased from Sigma Aldrich while hydrochloric acid was from Codec Chemical Co. Ltd.. E-glass fibers (manufactured by PPG Industries, trade name XG 2089) with a diameter of 16.0 ± 0.1 μm and an epoxy-compatible sizing were used as received. A bicomponent epoxy resin (epoxy base EC 252 and hardener W 241) was provided by Elantas Europe S.r.l. (Parma, Italy). The physical properties of epoxy resin cured at room temperature for 3h followed by 15h at 60°C are summarized in Table 1.

2.2 Preparation of graphene oxide and coating of glass fibers

Graphene oxide (GO) was synthesized using an approach derived from the Hummer's method [26] and described in [23]. The obtained brown solution was dried in a vacuum oven at 50 °C for at least 36 hours to obtain GO powder.

A schematic description of the electrophoretic deposition (EPD) process used to deposit GO nanosheets on glass fibers (GFs) is depicted in Figure 1. Initially, GO powder was dispersed in water (1 mg/ml) and the solution was subjected to bath-sonication for 1 hour. Since GFs are non-conductive, two copper plates were used as electrodes in the EPD process. Strands of GFs (fixed on a metallic window frame) were placed near the anode since GO display negative potential due to functionalities attached during the oxidation reaction. Hence, during the EPD process graphene oxide migrated towards the anode and deposited on the GFs. EPD was carried out under an applied voltage of 10

V/cm with a constant deposition time of 5 min and a gap between the electrodes of 2 cm. A second EPD cycle was performed under the same conditions while reversing the exposed side of GFs so that a homogenous deposition could be achieved on the fiber surface. The coated samples were dried in a vacuum oven at 40 °C for 12 hours. The selected experimental conditions have been optimized as reported in previous studies [23, 27] in order to maximize the interfacial fiber-matrix adhesion.
The dried fibers were exposed to hydrazine hydrate vapors at 100°C for 24 hours to reduce the GO coating to rGO [28].

2.3 Preparation of GF/rGO/epoxy single fiber model composites

Single rGO coated GF were axially aligned in a silicon mold in which the epoxy resin was poured to fabricate single-fiber model composites for testing the interfacial shear strength (ISS). Pre-curing of the epoxy resin for at least 3 hours at room temperature was performed before curing at 60 °C for 15 hours. The dimensions of each prismatic cured coupon were 50 mm × 5 mm × 2 mm. The ISS values of bare glass fibers and GO coated single fibers based epoxy composites were investigated under the same conditions in our previous work [23].

2.4 Preparation of hybrid epoxy/glass high fiber volume fraction composites

Hybrid epoxy/glass composites consisting of GO and rGO coated glass fibers were created by hand lay-up method. Briefly, laminates of coated glass fibers were stacked over each other after wetting them with epoxy resin. A constant pressure of 10 KPa was applied on the laminate whose curing was obtained under the conditions described in section 2.3. The resulting composites had a fiber volume fraction of about 50% as determined by density measurements.

2.5 Testing methods

The oxidation level of pristine graphite, GO and rGO nanosheets was evaluated using X-ray diffraction. Tests were performed using a Rigaku III D-max diffractometer (monochromatic radiation Cu-Kα line with $\lambda = 51.54056$ Å) in the 2θ range from 5° to 60° with a step of 0.04°.

A Nikolet Avatar 330 device with a 4 cm^{-1} resolution was used to record Fourier transform infrared (FTIR) spectra. Pristine graphite, GO and rGO powders were individually mixed with potassium bromide (KBr) powder to form homogeneous mixtures and thin discs for analysis were compressed in a metal mold under a pressure of 1 MPa.

Elemental composition of GO and rGO nanosheets was analyzed by X-ray photoelectron spectroscopy (XPS) by a Kratos Axis Ultra DLD machine equipped with a hemispherical analyzer and a monochromatic Al Kα (1486.6 eV) x-ray source. A 90° emission angle between the axis of the analyzer and the sample surface was adjusted. O 1s and C 1s core lines of each sample were collected. The quantification, reported as relative elemental percentage, was performed using the integrated area

of the fitted core lines, after Shirley background subtraction, and correcting for the instrument sensitivity factors.

Field emission scanning electron microscopy (FESEM) observations were performed with a Zeiss SUPRA 40 microscope to analyze the morphology and coatings of graphene nanosheets on glass fibers. Approximately 5 nm thick layer of platinum was deposited on samples prior to FESEM observations.

Single-fiber fragmentation test (SFFT) was performed using a small tensile tester (Minimat, by Polymer Laboratories, Loughborough, UK) located under a polarized optical stereo-microscope (Wild M3Z by Leica) to monitor the fiber fragmentation process. Tensile tests were performed at a cross-head speed of 10 mm/min up to a strain of 10% for assuring the saturation of the fragmentation process. The mean fiber length at saturation, L_s, was measured on the optical micrographs by an image analysis software (Image J). A simplified micromechanical model proposed by Kelly and Tyson [34] was utilized to derive the ISS values. According to Kelly and Tyson, a critical fiber length value, L_c, was considered to be $4/3\,L_s$. The static equilibrium between the tensile force acting on a fiber and the shear force transferred through the fiber-matrix interface allow one to determine an average value of ISS according to the following equation:

$$ISS = \frac{\sigma_{fb}(L_c)\,d}{2L_c} \qquad \text{(Eqn. 1)}$$

where d is the fiber diameter and $\sigma_{fb}(L_c)$ is the tensile strength of the fiber at the critical length. This latter value can be estimated by assuming a two-parameters Weibull distribution for the fiber strength, i.e.:

$$\sigma_{fb}(\mathrm{L_C}) = \sigma_0 \left(\frac{\mathrm{L_C}}{\mathrm{L_0}}\right)^{-\frac{1}{\mathrm{m}}} \Gamma\left(1+\frac{1}{\mathrm{m}}\right) \qquad \text{(Eqn. 2)}$$

where σ_0 and m are respectively the scale and shape parameters of the Weibull strength distribution at the reference length L_o, whereas Γ is the Gamma function. These parameters were assessed from tensile tests performed on single fibers. Particularly, single filaments of fiber were extracted from a strand and tested in agreement to the ASTM standard C1557 by using an Instron 4502 universal tensile tester equipped with a 10 N load cell. A gage length of 20 mm was used and 0.2 mm/min of cross-head speed was applied. An iterative procedure originally proposed by Gurvich et al. [35] was used for the data reduction whose outcome is summarized in Table 2.

The following mechanical tests were performed on the laminates by using an Instron 5969 electromechanical testing machine equipped with a 50 kN load cell.

1) Three-point bending tests were performed according to ASTM D790 on specimens with dimensions of around 80 mm × 13 mm × 1 mm, while the span to depth ratio was fixed at 60:1 and 40:1 for determining flexural modulus and flexural strength, respectively. Therefore, in order to maintain a strain rate of 0.01 mm^{-1}, cross-head speeds of 6.9 mm/min for flexural modulus evaluation and 3.1 mm/min for flexural strength evaluation were respectively adopted.

2) Short beam shear test was performed according to ASTM D2344 standard. At least 5 specimens 4 mm thick were tested under three-point bending at a cross-head speed of 1 mm/min until a deflection equal to the thickness of the specimen was achieved. The maximum corresponding force (F_m) value was used to evaluate the interlaminar shear strength as:

$$ILSS = 0.75 \times \frac{F_m}{b \times h}$$

3) Mode I fracture toughness test was performed according to the ASTM 5528 standard. The procedure involved creation of composite specimens consisting of 18 unidirectional laminae with a middle insert of Teflon thin film (thickness = 23 μm) which acted as a crack starter. The final dimensions of the specimen were around 180 mm × 25 mm × 4 mm. Piano hinges were attached to the composite specimen 50 mm apart from the crack tip. The crack advancement during the test was monitored using a digital webcam (Logitech B910 HD) that recorded the video in synchronization with the loading test. Three specimens for each sample were tested at a cross-head speed of 2.5 mm/min and the results were analyzed by considering the following three different criteria. i) Deviation from linearity (NL) was obtained by considering the point in load-displacement plot where deviation from linearity was observed (or onset of nonlinearity NL), assuming the delamination starts to grow from the insert. ii) Visual observation (VIS) point where the delamination was visually observed to grow from the insert. iii) Maximum load (MAX), the highest load measured during the test as obtained from the load-displacement plot.

The short term creep response was investigated by a TA instruments DMA Q800 device in dual cantilever mode. Prismatic specimens of dimensions 55 mm × 13mm × 1.3 mm were tested under a constant stress (σ_0) of 5MPa at 30°C for 3600 s.

Two different methods were employed for resistivity measurement depending on the electrical behavior of the investigated materials. For specimens having electrical resistivity levels exceeding 10^6 Ωcm, the measurements were performed by using a Keithley 8009 resistivity test chamber coupled with a Keithley 6517A high-resistance meter. For more conductive samples, a 6-1/2-digit

electrometer/high resistance system (Keithley model 6517A) was used and a 2-points electrical measurement was chosen as test configuration.

3 Results and Discussion

3.1 Microstructural characterization

As reported in Figure 2, X-ray diffraction patterns of precursor graphite show a characteristic and intense peak (0 0 2) at 26.4° thus revealing the crystalline nature of pristine graphite powder. Due to oxidation reaction of graphite powder, the (002) peak is replaced by a (001) diffraction peak of GO. The peak shift is due to the increase in interlayer spacing of graphite layers because of insertion of oxygen functional groups in GO as well as water molecules [29, 30]. Finally, the rGO diffractogram manifests a peak repositioned back to the pristine graphite peak location due to the removal of most of the oxygen groups from GO, hence decreasing the interlayer spacing. Note that both GO and rGO peaks are less intense and broader due to amorphous/distorted nature hence confirming exfoliation.

FTIR spectra of graphite, GO and rGO are reported in Figure 3. As compared to pristine graphite, GO shows relatively intense peaks of groups like epoxy C-O (at 1085 cm^{-1}), C=O (at 1625 cm^{-1}) and O-H (at 3830 cm^{-1}) that confirms the destruction of original extended conjugated π-orbital system of the graphite and insertion of oxygen-containing functional groups into carbon skeleton [31]. However, after chemical reduction, a lowering in the intensity of the functional groups peaks of rGO spectra can be observed, hence confirming the partial removal of oxygen-containing groups.

Figure 4 shows the XPS spectra of both GO and rGO samples. In brief, the C 1s XPS spectrum of GO indicates a certain degree of oxidation with at least three components of oxygen functional groups attached to carbon: the carboxyl group (COOH), the C in C-O bonds and non-oxygenated carbon (C-C). The semi-qualitative results for the carbon and oxygen present on the specimen surface were also calculated using the atomic sensitivity factors which showed oxygen and carbon levels of 34% and 66% respectively (Table 3). XPS spectrum of rGO also displays the same functional groups present in the sample however the difference is the reduced intensity of peaks of oxygenated groups while the non-oxygenated carbon group had a higher intensity. The presence of a new group such as C-N in rGO spectrum is related to the fact that the chemical reduction of GO was obtained by exposure to hydrazine hydrate vapors having nitrogen as a key element. After chemical reduction, the amount of oxygen in rGO decreases to 9.9% (Table 3).

SEM pictures reported in Figure 5 display the surfaces of GF fibers extracted from a bundle before (Figure 5a) and after (Figures 5b)EPD coating with GO and subsequent chemical reduction of the coating to rGO (Figures 5c) nanosheets. Figures 5b and 5c clearly show that the glass fibers

are completely covered with GO and rGO nanosheets thus confirming the efficacy of the proposed electrophoretically deposition method [23, 32].

A detailed study of the interaction between a coating of GO electrophoretically deposited onto E-glass and subsequently reduced into rGO by exposure to hydrazine hydrate at 100°C fiber has been recently performed [33]. Treatment with hydrazine hydrate reduces adhesion and friction force against diamond like carbon coated Si probe (DLC AFM) at the basal plain of the coatings. Investigation at the edges revealed that the presence of oxygen functional group leads to higher shear strength with glass-fiber which reduces after treatment with hydrazine.

3.2 Fiber-matrix adhesion in single-fiber model composites

The average values of fiber's fragment lengths measured in SFFT and subsequent calculations of ISS for rGO coated glass fibers epoxy composite and their comparison with uncoated and GO coated glass fiber epoxy composites are reported in Table 4. rGO coated fibers show a decrease of the fragments length at saturation as compared to uncoated ones. This naturally brings to estimate higher ISS values. ISS values measured with both GO and rGO coated fibers are higher than those obtained with uncoated GF. The enhancement of ISS for GO and rGO coated fibers as compared to uncoated fiber could be attributed to the fact that both GO and rGO contain functional groups which provide a possibility of favorable bond between the GFs and epoxy resin which eventually enhances the effective distribution of load on the GF. Another reason for an increase in ISS could be the increased surface roughness and the good adhesive compatibility between the epoxy matrix and the deposited coatings which promote mechanical interlocking. An important fact to be considered here is that this 70% increase observed for rGO coated fibers is lower than the previously reported increment percentage in case of GO coating [23]. This is due to the fact that rGO contains less functional groups which play a major role for a better adhesion and consequently improved load transfer mechanisms [34].

3.3 Mechanical behaviour of unidirectional composites

Typical flexural stress-strain curves of the multiscale composites are reported in Figure 6. It can be observed that the presence of both GO and rGO interphase improve the composites behaviour. Figure 7 shows the resulting flexural modulus and flexural strength values. The flexural modulus increases by 19% and 9% for GO and rGO coated GF, respectively, as compared to neat composites. The increase in modulus is related to the fact that GO interphase between the matrix and the fibers improved the bonding conditions and mechanical interlocking phenomena [23]. The flexural strength of the composites containing GO shows an increase by 20%, again due to the better interfacial

adhesion, but in case of rGO, the value is practically the same as compared to uncoated fiber based composites.

Interlaminar shear strength (ILSS) values of the composites was investigated by the short beam shear and the obtained values are reported in Figure 8. The epoxy/glass composites with a GO interphase reach a 15% increase in the ILSS as compared to composites with uncoated fibers while a 9% increase is found for rGO based glass/epoxy composites. This result also supports previous observations in which GO coated fibers offer dual reinforcing phenomena i.e. oxygen-based functional groups and mechanical interlocking together bridging the epoxy and glass fibers in the composite [23]. This "cross-linking" via the interface causes an enhancement in interfacial strength, which can be inferred as an evidence for the enhanced ILSS values. In case of rGO coated fibers, the main reinforcing mechanism is the mechanical interlocking which promotes an increase of ILSS but not at the levels observed for GO coated fibers. Again, the observed differences can be attributed to the lower amount of oxygen-based functional groups on the surface of rGO in comparison of rGO coated fibers. The images of the composite specimens failed during short beam shear test are reported in Figure 9 where the interlaminar failure can be clearly noticed. It is interesting to observe that the composite with rGO coated fibers (Figure 9c) presents more shear cracks between the laminae.

In case of Mode I fracture toughness tests, the strain energy release rate values for each composite are evaluated from the load-displacement plot of Figure 10a and plotted as resistance curves (R-curves) as shown in Figure 10b. Table 5 shows the average values of the three composites tested. An explanation of the obtained G_{Ic} values can be best provided by a comparison with the ILSS values as obtained from the short beam shear test. As it can be seen in Figure 10c, composites reinforced with GO coated GF showed the highest values for the NL and VIS G_{Ic} values as compared to uncoated GF and rGO coated GF. The G_{Ic} values computed according to the MAX procedure are however practically the same for the composites. rGO coated GF fibers also provide some resistance to crack propagation but less than GO coating, which is pretty comparable to the result of ILSS. This investigation clearly shows the higher energy required for crack propagation when GO is deposited on GF as a continuous reinforcing interphase in epoxy/glass composites.

Interesting observations were obtained during the analysis of the fracture surfaces obtained after mode I fracture toughness test of DCB specimens. The fracture surfaces of Ep-GF composite (Figure 11a) indicate a weak fiber-matrix interaction revealed by the presence of the glass fibers with a clean surface. On the other hand, the fracture surfaces of Ep-GO-GF (Figure 11b) shows a number of fibers coated with the remnants of epoxy matrix which could be associated to a good interfacial

adhesion. It can be visualized from the FESEM images that the fibers are bonded together with continuous epoxy resin hence suggesting the influence of GO coating on fibers promoting strong inter-fiber interactions due to epoxy/GO/GF system. At the end, the fracture surfaces obtained from the Ep-rGO-GF composite system gives a different picture in which the fiber surfaces are covered totally with a continuous coating (Figure 11c). A detail examination reveals that the rGO coating had a different morphology as compared to the epoxy matrix. The lower values of NL during mode I fracture toughness is a clear evidence that debonding took place at the epoxy/rGO interface. This is correlated to the fact that rGO sheets, due to unavailability of the oxygen based functional groups, offered a weaker interfacial adhesion towards the epoxy matrix.

The improvement in mechanical properties obtained in this work are summarized in Table 6 in which the results are also compared with recent work done for improving similar properties in other systems. It can be seen that the trend involves the use of graphene as an interphase thus creating a synergistic effect of improving of mechanical properties by the combination of chemical bonding plus mechanical interlocking between the matrix and the fiber.

Isothermal creep compliance curves of the unidirectional composites with uncoated, GO coated and rGO coated glass fibers at a reference temperature of 30°C and applied stress of 5 MPa are shown in Figure 12 while the values of the instantaneous creep compliance (De), of the viscoelastic component after 2000 s (D_{ve2000}) and of the total creep compliance after 2000 s (D_{t2000}) are reported in Table 7. A significant reduction of the creep compliance can be noticed for composites reinforced with GO and rGO coated fiber as compared to reference composite with uncoated fibers. This improvement in the creep stability is the consequence of a remarkable reduction of both the elastic and the viscoelastic components of the total creep compliance.

Findley's model was adopted to fit the experimental data obtained through creep testing. This model can be obtained by expanding the Kohlrausch–Williams–Watts (KWW) model, generally described by a Weibull-like function as a series and ignoring all but the first term [35]:

$$D(t) = D_0 + k(t)^n \tag{1}$$

where D_0 is the elastic instantaneous creep compliance, k is a coefficient related to the magnitude of the underlying retardation process and n is an exponent tuning the time dependency of the creep process. D_0 and k are functions of environmental variables. In this work, creep curves at different temperatures for different composites were fitted using Findley's model to investigate possible correlations between the viscoelastic response of the material and the fitting parameters. The creep compliance curves of the investigated composites have been tentatively fitted with the Findley model

(Equation 1), and the results are shown in Figure 12. The parameters obtained from the best fitting of experimental creep data are summarized in Table 7, along with R^2 values. It can be noticed that the Findley model successfully fits all the creep curves, with R^2 values of around 0.99 for all the cases. It is interesting to observe that, as compared to neat composites, the reduction of the creep compliance due to the presence of the GO coating in Ep-GO-GF composites results in a substantial reduction of the instantaneous creep compliance term D_e and of the coefficient k, related to the strain retardation process of the macromolecules. Moreover, the parameter n was not changed by the GO coating of the GF as compared to the uncoated GF based epoxy composite. For Ep-rGO-GF composite, however, there was a slight increase of the D_e as compared to the neat composite and at the same time the coefficient k drops very significantly, which shows that the retardation of creep process increases tremendously afterwards.

3.4 Electrical resistivity and piezoresistivity behaviour

Three different composites were tested for their electrical resistivity as shown in Figure 13. In case of uncoated glass fibers/epoxy composite (GF/Ep), the volume resistivity is in the range of 10^{14} Ω cm which is a typical value for insulating epoxy/glass composites. When composites are prepared by using glass fibers coated with GO only a small decrease of the electrical resistivity is observed with volume resistivity value in the range of 10^{13} Ω cm, this being due to the insulating nature of GO [36]. However, for the composite with an rGO interphase a volume resistivity value as low as 10^2 Ω cm can be measured. The massive drop in resistivity thus confirms the reduction of GO and hence making the graphene sheets conductive.

The piezoresistive response of GF/rGO/Ep composites was monitored on composite specimens subjected to mechanical loading and a simultaneous measure of electrical resistance by two points contact. Figures 14, 15, 16 and 17 show the dependence of electrical resistance on the applied strain (or stress) for the GF/rGO/Ep composites under various loading modes. In case of quasi-static tensile mode (as schematically depicted in Figure 14a), it is interesting to observe that within the initial 0.1% strain (Figure 14b), the electrical resistance decreases which could be attributed to the rearrangement of the coated fibers at the microscale hence a possibility of having better electrical coupling among each other consequently a decrease in resistance. At higher strain levels, the change in resistance increases steadily till it became steep after 0.2% tensile strain. Considering this, a tangent line in this elastic portion provide a gage factor of about 11 by the formula $\left(k = \left(\Delta R / \mathrm{R}_0\right) / \varepsilon\right)$. Since the Poisson's ratio of the analyzed composite was 0.36 (as measured by a biaxial extensometer), the contribution of the geometric part can be estimated to be of about 0.01. Figure 15a shows the schematic diagram of the flexural test wherein the piezoresistivity was monitored on the bottom side of the specimen which experiences the tensile stresses. In Figure 15b

the piezoresistivity response of the specimen's surface under tensile stress is reported. The piezoresistivity on this surface could be visualized when considering the influence of stresses acting on the fibers. A steady resistance change can be observed till 2.5% of flexural strain, the resistance change was steady until the fibers started to break resulting in failing of the specimen which consequently had a dramatic effect on the relative change of resistance. Similar kind of behavior can be also observed from the analysis of the compressive side of the specimen (Figure 15c, Figure 15d).

In another testing protocol, the reversibility of electrical network was tested by subjecting the hybrid composite specimen under repeated loading-unloading cycles in the strain range of $0.1\% < \varepsilon < 0.5\%$ and the electrical resistance was monitored during each loading and unloading part of the cycle. Figure 16 shows the results obtained under cyclic tensile conditions in which the reversible piezoresistivity can be confirmed. The gage factor calculated here was about 3.8. A similar test method was also applied to load a specimen under cyclic flexural mode under load control (0-25 MPa). As shown in Figure 17, the piezoresistive behavior the multiscale composite is also replicated in flexural mode which confirms the rGO coating on GF can provide the possibility of a strain monitoring based on the control of the electrical resistance variations.

4 Conclusions

GO was successfully deposited on GF using electrophoretic deposition technique and subsequently reduced to rGO using hydrazine hydrate at 100°C for 24 h. XPS analysis evidenced a reduction of the oxygen content from 34.2% of GO to 9.9% of rGO. The obtained rGO coating appeared to be quite uniform across a length of fiber.

Fiber-matrix interfacial adhesion evaluated by single fiber fragmentation test on epoxy matrix showed a +70% increase in ISS of rGO based epoxy/glass composites as compared to uncoated GF based composites. This ISS is lower than the increase (+218%) measured on composites with GO coated fibers due to less oxygen based functional groups attached with rGO nanosheets. Mechanical test (three-point bending, short beam shear and mode-I fracture toughness) on high fiber volume fraction composites revealed that GO coted fibers lead to an increase of elastic modulus, stress at break and interlaminar shear strength, while composites with rGO coated fibers perform similarly to composites with uncoated fibers. In addition, short term creep tests revealed how a graphene-based interphase offers excellent resistance to creep deformation.

Finally, composites possessing rGO interphase manifested low resistivity values due to the conductive nature of rGO nanosheets. Piezoresistivity of the rGO based composites was verified by

applying various loading conditions and simultaneously measuring changes in electrical resistance hence confirming the applicability of such composites for strain monitoring in structural applications.

References

[1] Pegoretti A, Karger-Kocsis J. Interphase engineering in polymer composites: Challenging the devil…. Express Polymer Letters. 2015;9(10):838.

[2] Jones FR. A Review of Interphase Formation and Design in Fibre-Reinforced Composites. Journal of Adhesion Science and Technology. 2010;24(1):171-202.

[3] Karger-Kocsis J, Mahmood H, Pegoretti A. Recent advances in fiber/matrix interphase engineering for polymer composites. Progress in Materials Science. 2015;73:1-43.

[4] Gupta RK, Kennel E, Kim K-J. Polymer Nanocomposites Handbook. Boca Raton, FL: CRC Press; 2010.

[5] Sun X, Sun H, Li H, Peng H. Developing Polymer Composite Materials: Carbon Nanotubes or Graphene? Advanced Materials. 2013;25(37):5153-76.

[6] Inpil K, Mark JS, Jay HK, Vesselin S, Donglu S. A carbon nanotube strain sensor for structural health monitoring. Smart Materials and Structures. 2006;15(3):737.

[7] Zhang W, Suhr J, Koratkar N. Carbon Nanotube/Polycarbonate Composites as Multifunctional Strain Sensors. Journal of Nanoscience and Nanotechnology. 2006;6(4):960-4.

[8] Böger L, Wichmann MHG, Meyer LO, Schulte K. Load and health monitoring in glass fibre reinforced composites with an electrically conductive nanocomposite epoxy matrix. Composites Science and Technology. 2008;68(7–8):1886-94.

[9] Moriche R, Sánchez M, Jiménez-Suárez A, Prolongo SG, Ureña A. Strain monitoring mechanisms of sensors based on the addition of graphene nanoplatelets into an epoxy matrix. Composites Science and Technology. 2016;123:65-70.

[10] Moriche R, Sánchez M, Prolongo SG, Jiménez-Suárez A, Ureña A. Reversible phenomena and failure localization in self-monitoring GNP/epoxy nanocomposites. Composite Structures. 2016;136:101-5.

[11] Ferrari AC, Bonaccorso F, Fal'ko V, Novoselov KS, Roche S, Boggild P, et al. Science and technology roadmap for graphene, related two-dimensional crystals, and hybrid systems. Nanoscale. 2015;7(11):4598-810.

[12] Novoselov KS, Geim AK, Morozov SV, Jiang D, Zhang Y, Dubonos SV, et al. Electric field effect in atomically thin carbon films. Science. 2004;306(5696):666-9.

[13] Lee C, Wei X, Kysar JW, Hone J. Measurement of the Elastic Properties and Intrinsic Strength of Monolayer Graphene. Science. 2008;321(5887):385-8.

[14] Balandin AA, Ghosh S, Bao W, Calizo I, Teweldebrhan D, Miao F, et al. Superior Thermal Conductivity of Single-Layer Graphene. Nano Letters. 2008;8(3):902-7.

[15] Kuilla T, Bhadra S, Yao D, Kim NH, Bose S, Lee JH. Recent advances in graphene based polymer composites. Progress in Polymer Science. 2010;35(11):1350-75.

[16] Park S, An J, Jung I, Piner RD, An SJ, Li X, et al. Colloidal Suspensions of Highly Reduced Graphene Oxide in a Wide Variety of Organic Solvents. Nano Letters. 2009;9(4):1593-7.

[17] Stankovich S, Dikin DA, Piner RD, Kohlhaas KA, Kleinhammes A, Jia Y, et al. Synthesis of graphene-based nanosheets via chemical reduction of exfoliated graphite oxide. Carbon. 2007;45(7):1558-65.

[18] Chang L, Friedrich K. Enhancement effect of nanoparticles on the sliding wear of short fiber-reinforced polymer composites: A critical discussion of wear mechanisms. Tribology International. 2010;43(12):2355-64.

[19] Pedrazzoli D, Pegoretti A. Expanded graphite nanoplatelets as coupling agents in glass fiber reinforced polypropylene composites. Composites Part A: Applied Science and Manufacturing. 2014;66:25-34.

[20] Vlasveld DPN, Parlevliet PP, Bersee HEN, Picken SJ. Fibre–matrix adhesion in glass-fibre reinforced polyamide-6 silicate nanocomposites. Composites Part A: Applied Science and Manufacturing. 2005;36(1):1-11.

[21] Dorigato A, Pegoretti A, Quaresimin M. Thermo-mechanical characterization of epoxy/clay nanocomposites as matrices for carbon/nanoclay/epoxy laminates. Mat Sci Eng a-Struct. 2011;528(19-20):6324-33.

[22] Chen J, Zhao D, Jin X, Wang C, Wang D, Ge H. Modifying glass fibers with graphene oxide: Towards high-performance polymer composites. Composites Science and Technology. 2014;97:41-5.

[23] Mahmood H, Tripathi M, Pugno N, Pegoretti A. Enhancement of interfacial adhesion in glass fiber/epoxy composites by electrophoretic deposition of graphene oxide on glass fibers. Composites Science and Technology. 2016;126:149-57.

[24] Ali MA, Umer R, Khan KA, Samad YA, Liao K, Cantwell W. Graphene coated piezo-resistive fabrics for liquid composite molding process monitoring. Composites Science and Technology. 2017;148(Supplement C):106-14.

[25] Moriche R, Jiménez-Suárez A, Sánchez M, Prolongo SG, Ureña A. Graphene nanoplatelets coated glass fibre fabrics as strain sensors. Composites Science and Technology. 2017;146(Supplement C):59-64.

[26] Hummers WS, Offeman RE. Preparation of Graphitic Oxide. Journal of the American Chemical Society. 1958;80(6):1339-.

[27] Pegoretti A, Mahmood H, Pedrazzoli D, Kalaitzidou K. Improving fiber/matrix interfacial strength through graphene and graphene-oxide nano platelets. IOP Conference Series: Materials Science and Engineering. 2016;139:1-12.

[28] Watcharotone S, Dikin DA, Stankovich S, Piner R, Jung I, Dommett GHB, et al. Graphene−Silica Composite Thin Films as Transparent Conductors. Nano Letters. 2007;7(7):1888-92.

[29] Buchsteiner A, Lerf A, Pieper J. Water dynamics in graphite oxide investigated with neutron scattering. The Journal of Physical Chemistry B. 2006;110(45):22328-38.

[30] Pan D, Wang S, Zhao B, Wu M, Zhang H, Wang Y, et al. Li Storage Properties of Disordered Graphene Nanosheets. Chemistry of Materials. 2009;21(14):3136-42.

[31] Lian P, Zhu X, Liang S, Li Z, Yang W, Wang H. Large reversible capacity of high quality graphene sheets as an anode material for lithium-ion batteries. Electrochimica Acta. 2010;55(12):3909-14.

[32] Chavez-Valdez A, Shaffer MSP, Boccaccini AR. Applications of Graphene Electrophoretic Deposition. A Review. The Journal of Physical Chemistry B. 2012;117(6):1502-15.

[33] Tripathi M, Mahmood H, Novel D, Iacob E, Vanzetti L, Bartali R, et al. Nanoscale friction of graphene oxide over glass-fibre and polystyrene Composites Part B: Engineering. submitted.

[34] Pei S, Cheng H-M. The reduction of graphene oxide. Carbon. 2012;50(9):3210-28.

[35] Dorigato A, Pegoretti A. Tensile creep behaviour of polymethylpentene–silica nanocomposites. Polymer International. 2010;59(6):719-24.

[36] Rao S, Upadhyay J, Das R. 8 - Manufacturing and characterization of multifunctional polymer-reduced graphene oxide nanocomposites A2 - Dong, Yu. In: Umer R, Lau AK-T, editors. Fillers and Reinforcements for Advanced Nanocomposites: Woodhead Publishing; 2015. p. 157-232.

[37] Chen L, Jin H, Xu Z, Shan M, Tian X, Yang C, et al. A design of gradient interphase reinforced by silanized graphene oxide and its effect on carbon fiber/epoxy interface. Materials Chemistry and Physics. 2014;145(1–2):186-96.

[38] Qin W, Vautard F, Drzal LT, Yu J. Mechanical and electrical properties of carbon fiber composites with incorporation of graphene nanoplatelets at the fiber–matrix interphase. Composites Part B: Engineering. 2015;69:335-41.

[39] Zhang RL, Gao B, Du WT, Zhang J, Cui HZ, Liu L, et al. Enhanced mechanical properties of multiscale carbon fiber/epoxy composites by fiber surface treatment with graphene oxide/polyhedral oligomeric silsesquioxane. Composites Part A: Applied Science and Manufacturing. 2016;84:455-63.

[40] Deng C, Jiang J, Liu F, Fang L, Wang J, Li D, et al. Effects of electrophoretically deposited graphene oxide coatings on interfacial properties of carbon fiber composite. Journal of Materials Science. 2015;50(17):5886-92.

[41] Zhang X, Fan X, Yan C, Li H, Zhu Y, Li X, et al. Interfacial Microstructure and Properties of Carbon Fiber Composites Modified with Graphene Oxide. ACS Applied Materials & Interfaces. 2012;4(3):1543-52.

Captions of Figures

Figure 1. Schematic diagram of the setup adopted for the electrophoretic deposition of GO nanosheets onto glass fibers.

Figure 2. X-ray diffractograms of graphite, GO and rGO.

Figure 3. Fourier transform infrared (FTIR) spectra of graphite, GO and rGO.

Figure 4. The C1s XPS spectra of GO and rGO.

Figure 5. Scanning electron microscopy images of a) bare glass fiber and b) glass fiber coated with GO and c) glass fiber coated with rGO.

Figure 6. Typical flexural stress-strain curves of unidirectional composites with uncoated, GO coated and rGO coated glass fibers.

Figure 7. a) Flexural modulus and b) flexural strength as determined by three-point bending tests on unidirectional composites with uncoated, GO coated and rGO coated glass fibers.

Figure 8.: Interlaminar shear strength (ILSS) values as obtained from the short beam shear tests performed on unidirectional composites with uncoated, GO coated and rGO coated glass fibers.

Figure 9. Optical microscopy images of composite specimens (side view) after being subjected to short beam shear tests: composites with a) uncoated, b) GO coated and c) rGO coated glass fibers.

Figure 10. a) Typical load-displacement curves obtained under mode I fracture toughness tests of investigated composites. b) Delamination resistance curves (R-curves) where half-filled symbols represent NL (Non linearity) and solid symbols represent VIS (visual observation). c) Comparison between mode I fracture toughness values (NL: non-linear, VIS: visual observation, MAX: maximum load, ILSS: interlaminar shear strength) and short beam shear strength.

Figure 11. Fracture surfaces of composites obtained during Mode I fracture toughness test as observed by FESEM (crack propagation from top to bottom) where a) Ep-GF, b) Ep-GO-GF and c) Ep-rGO-GF.

Figure 12. Experimental creep compliance curves (solid line) of the investigated composites and theoretical prediction (open circles) according to the Findley model (T = 30°C, σ = 5 MPa).

Figure 13. Volume resistivity of the unidirectional composites with uncoated, GO coated and rGO coated glass fibers.

Figure 14. a) Schematic of testing setup for piezoresistivity tests under tensile mode, b) piezoresistivity response of unidirectional composites with rGO coated glass fibers under tensile loading condition.

Figure 15. Schematic of testing setup for piezoresistivity tests under flexural mode where change in resistance was monitored on the surfaces experiencing a) tensile and c) compressive stresses, respectively. Piezoresistivity response of unidirectional composites with rGO coated glass under on the b) tensile and d) compressive sides of the specimens.

Figure 16. Piezoresistivity response of unidirectional composites with rGO coated glass fibers under tensile cyclic tests under strain control.

Figure 17. Piezoresistivity response of unidirectional composites with rGO coated glass fibers under flexural cyclic tests under load control.

Figure 1.

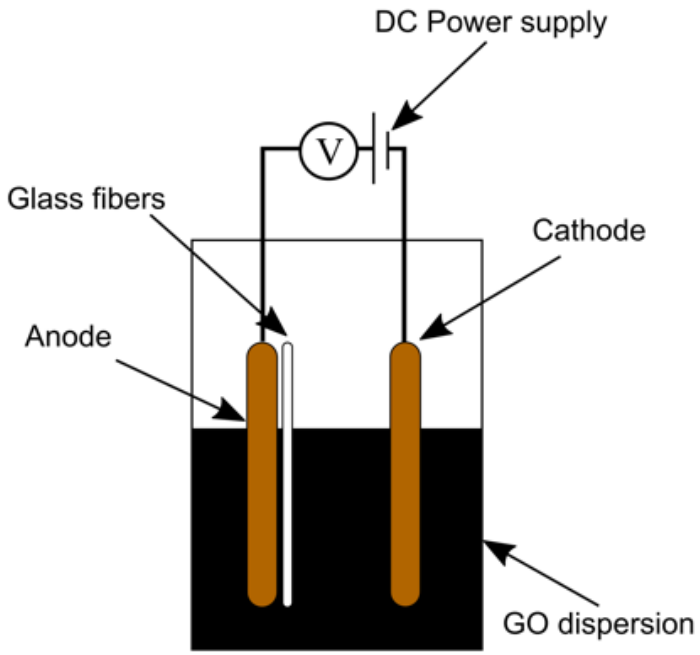

Figure 2.

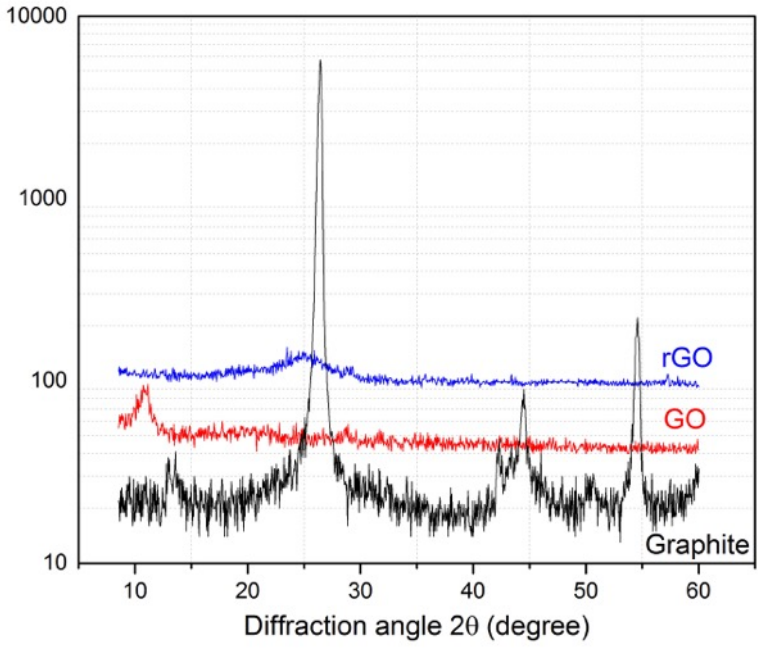

Figure 3.

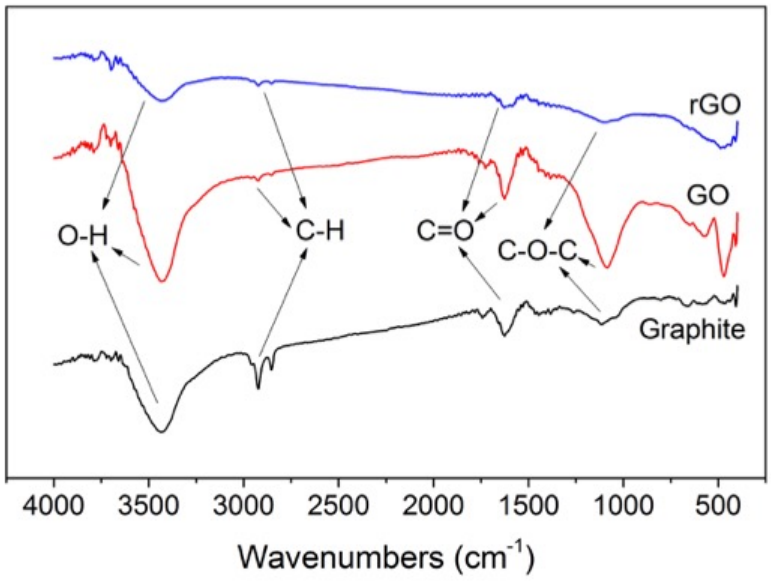

Figure 4.

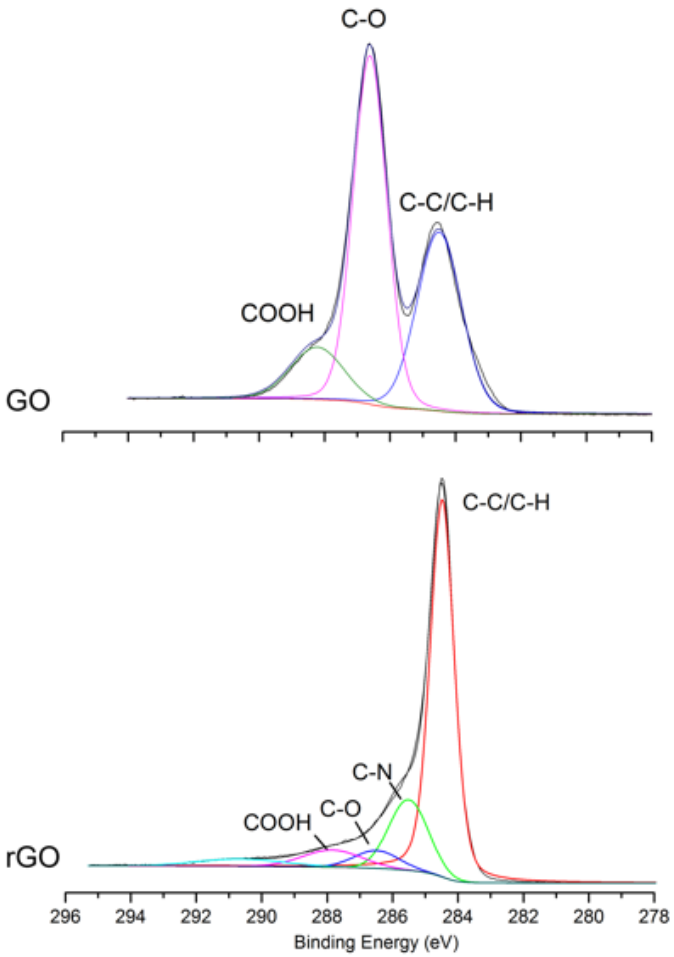

Figure 5.

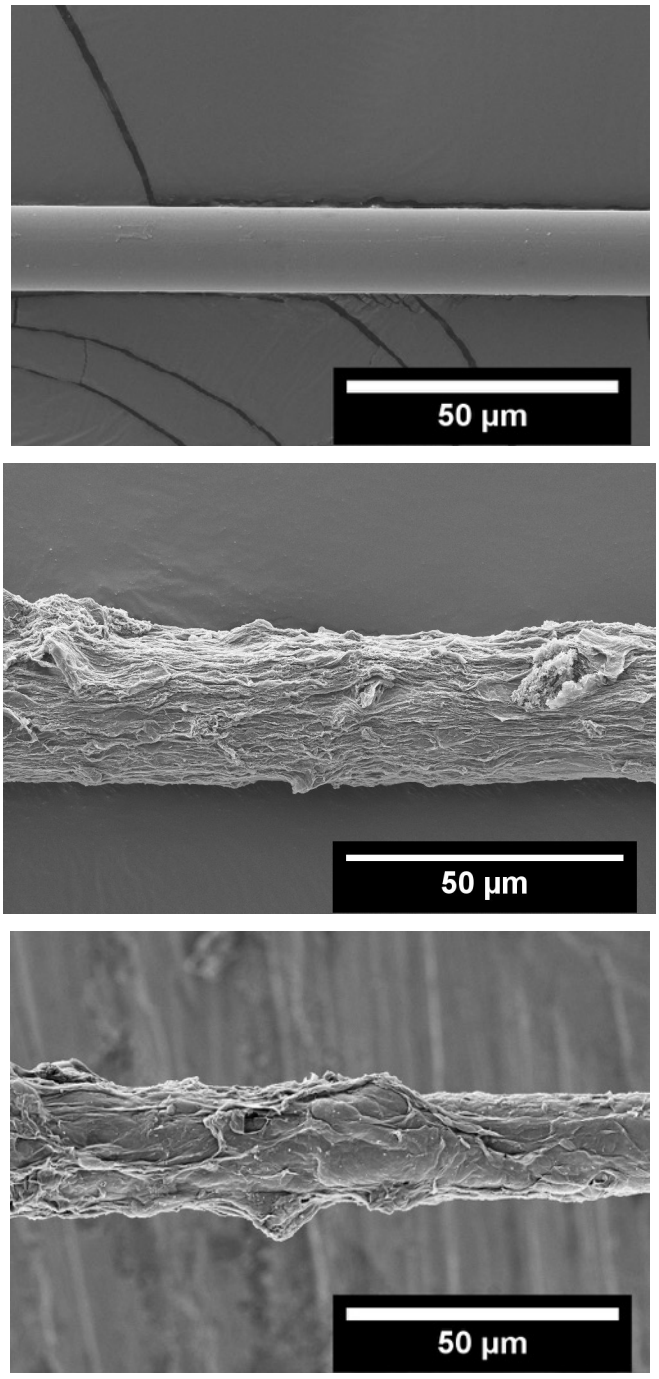

Figure 6.

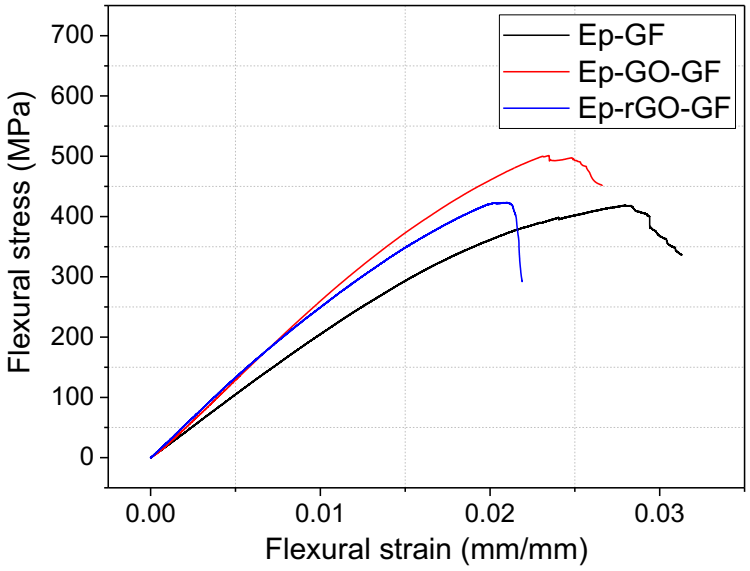

Figure 7.

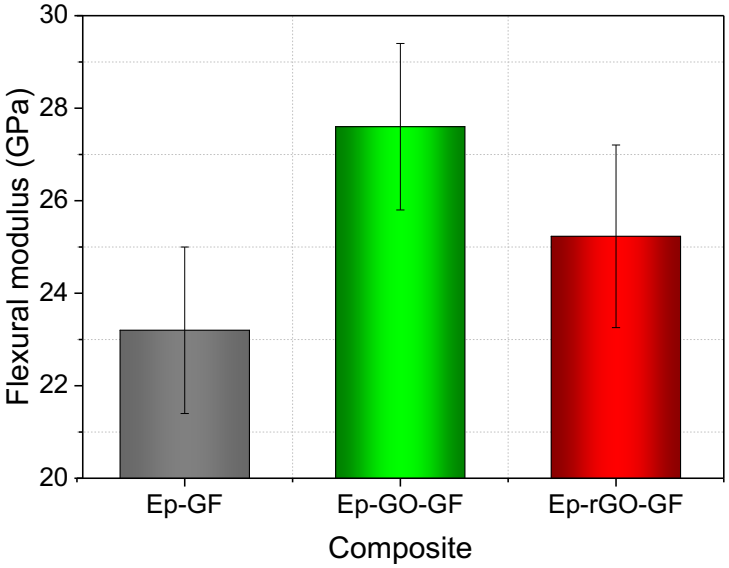

a)

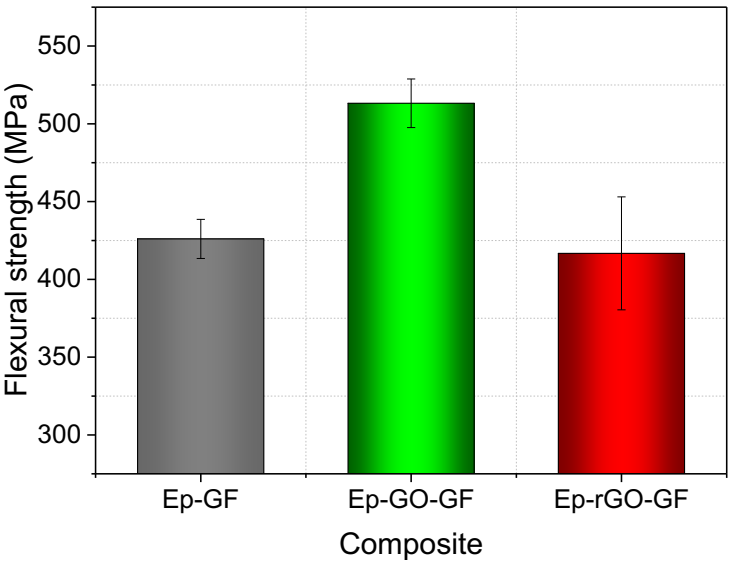

b)

Figure 8.

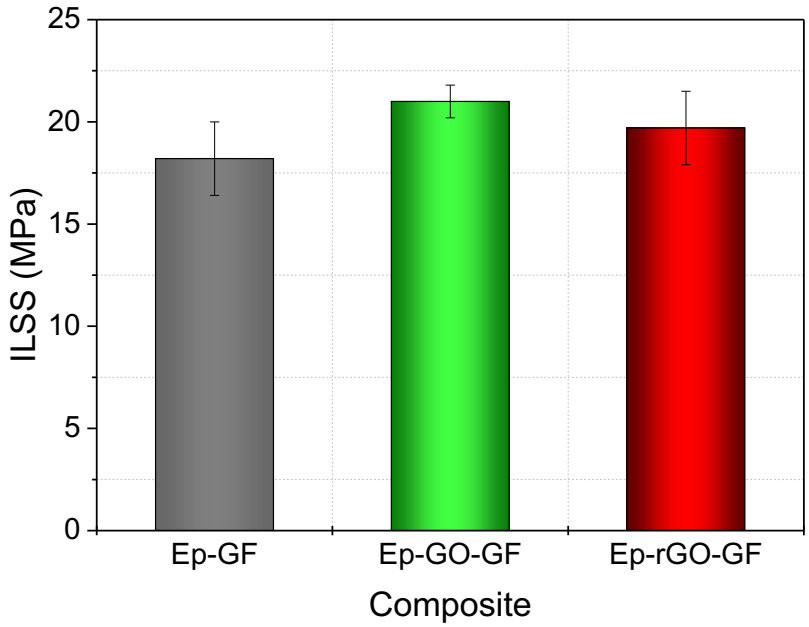

Figure 9.

a)

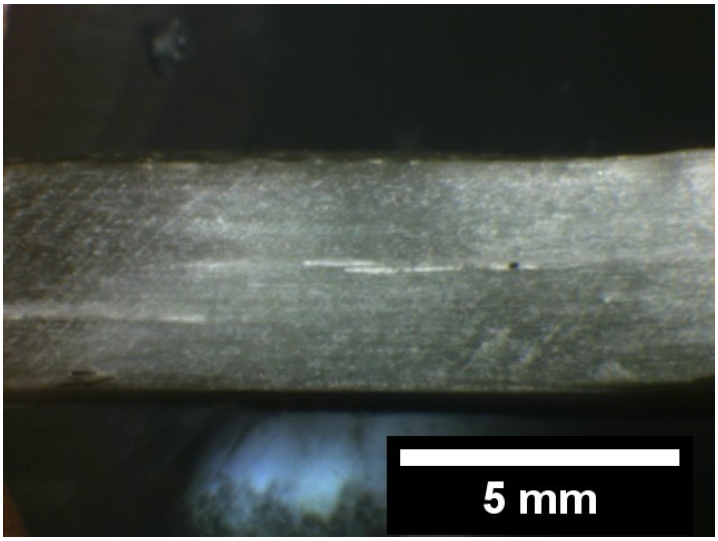

b)

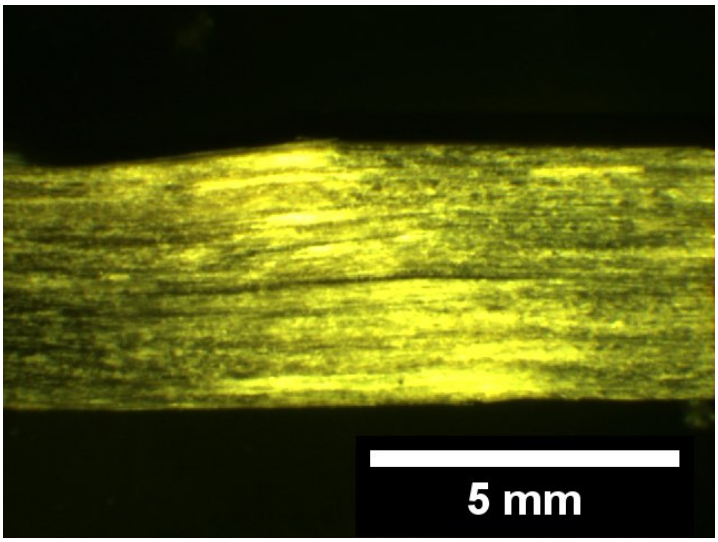

c)

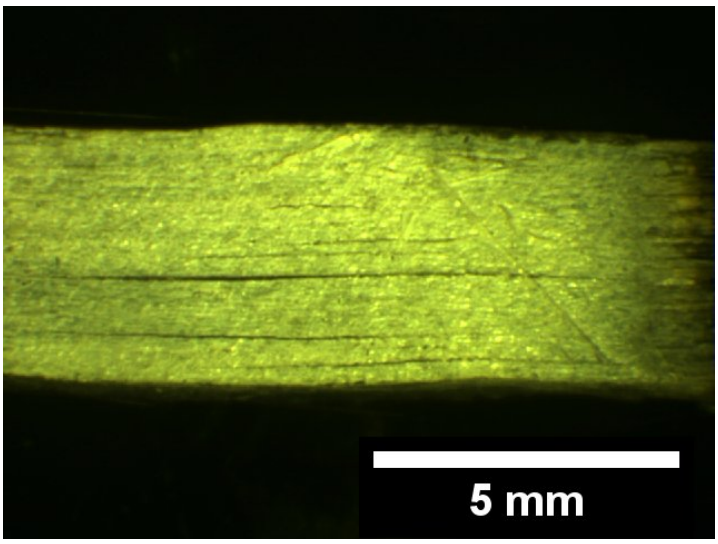

Figure 10.

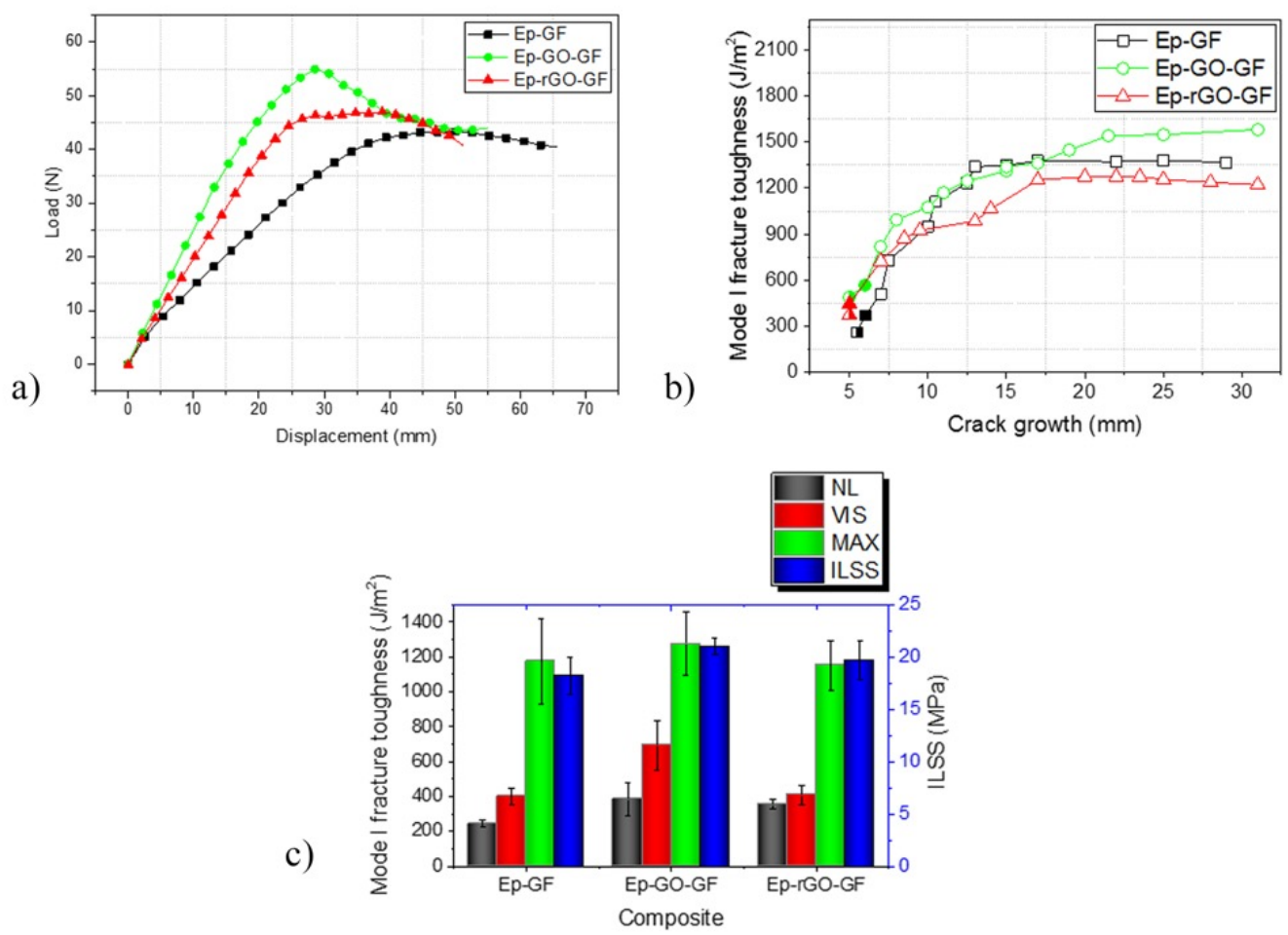

Figure 11.

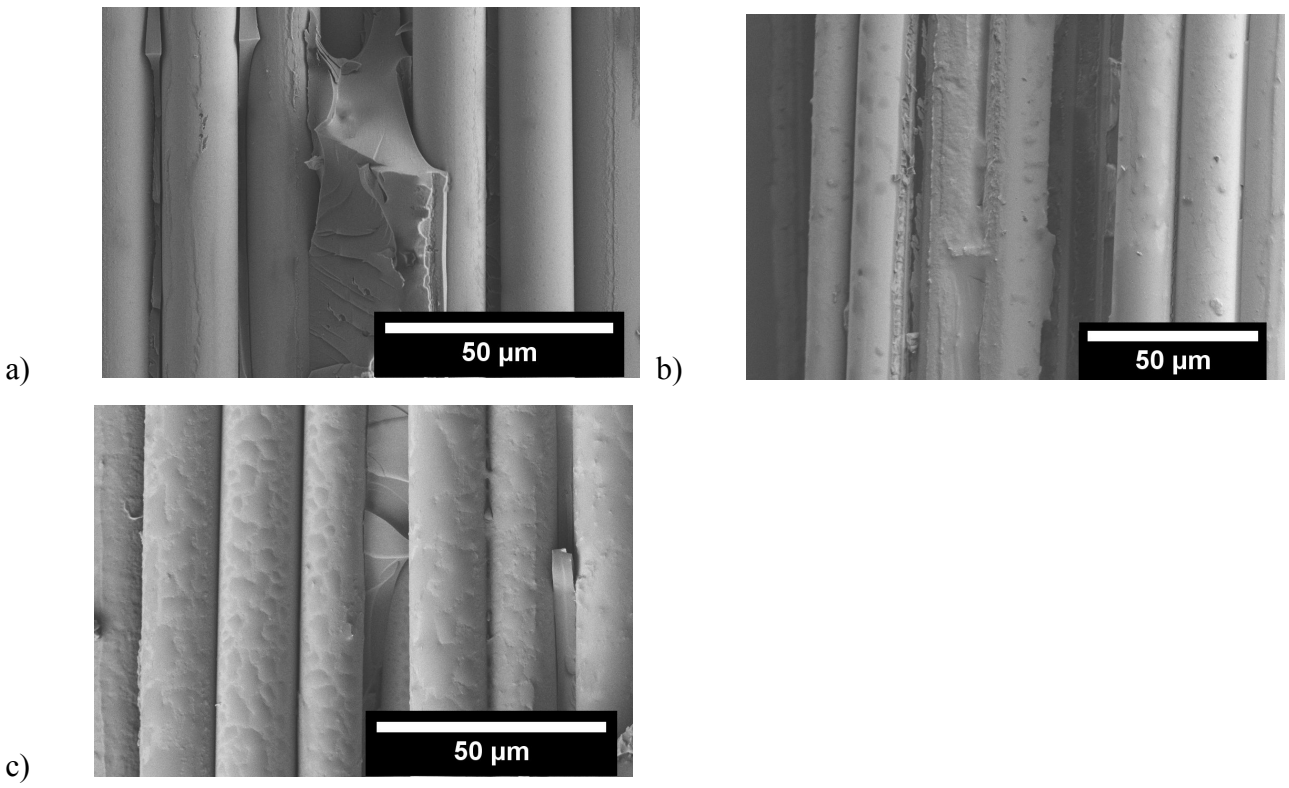

Figure 12.

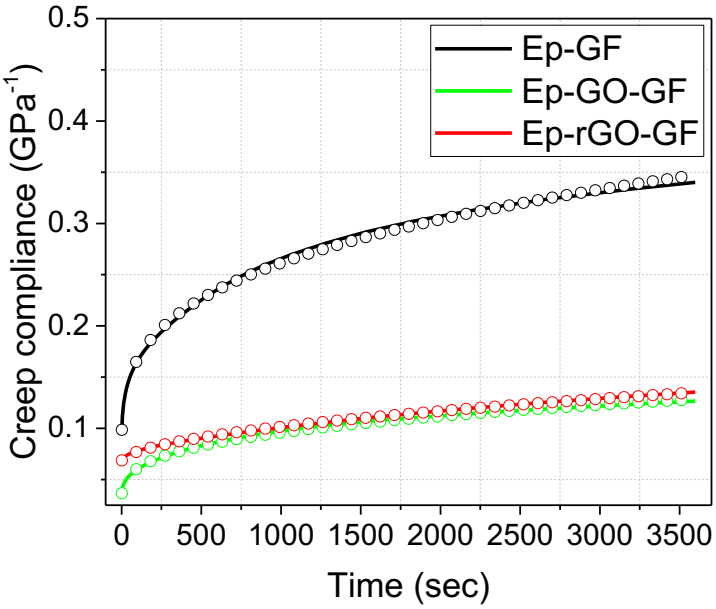

Figure 13.

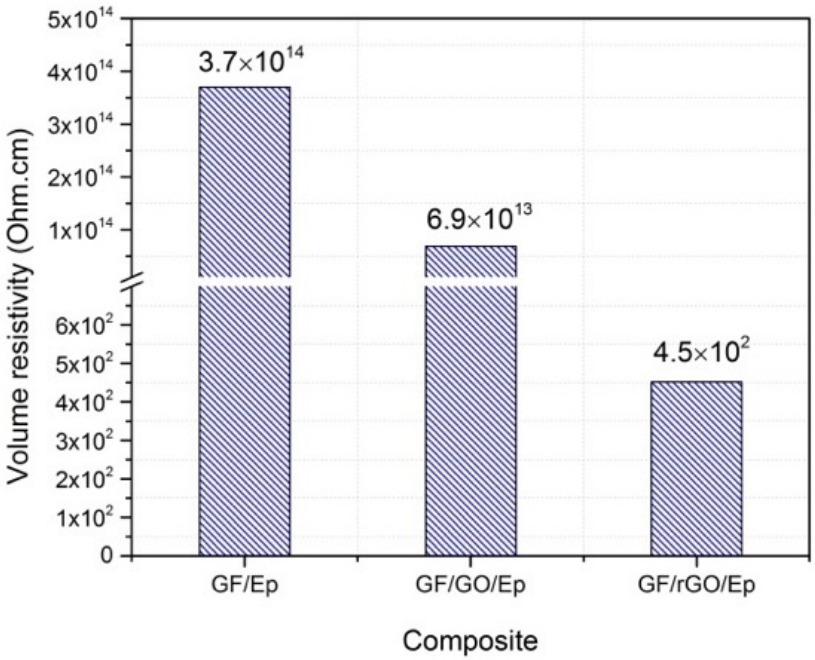

Figure 14.

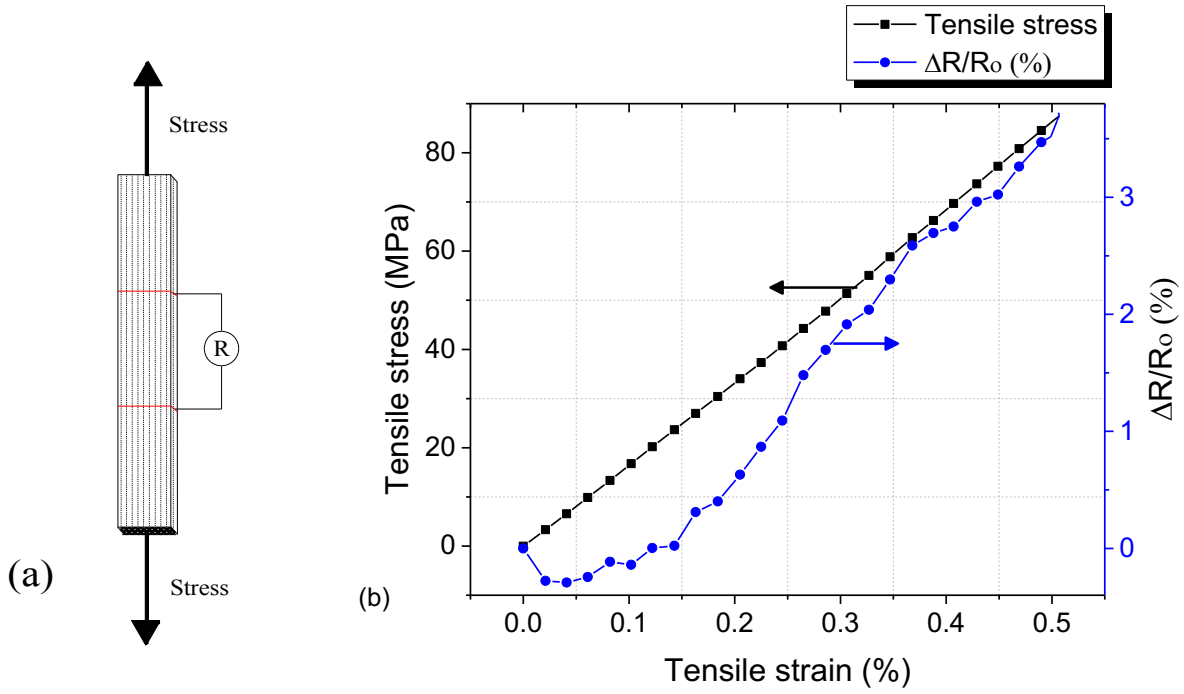
Stress
R
Stress
(a)
Tensile stress
ΔR/Ro (%)
Tensile stress (MPa)
ΔR/Ro (%)
Tensile strain (%)
(b)
0
20
40
60
80
0
1
2
3
0.0
0.1
0.2
0.3
0.4
0.5

Figure 15.

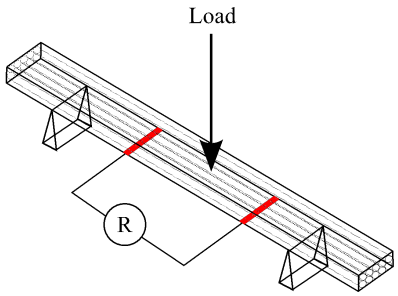

a)

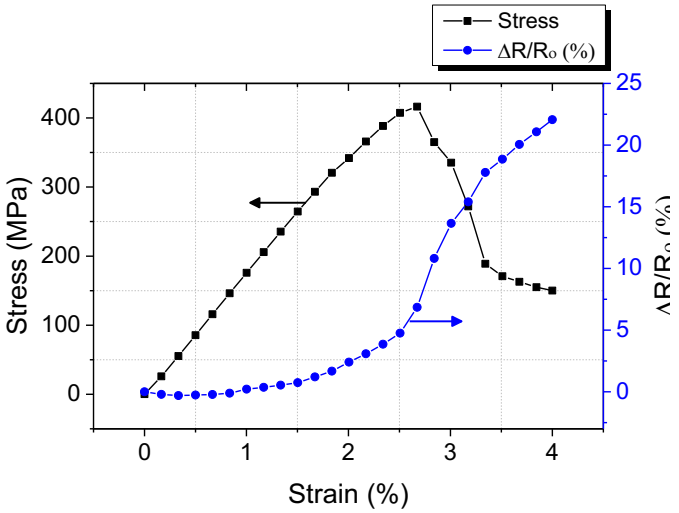

b)

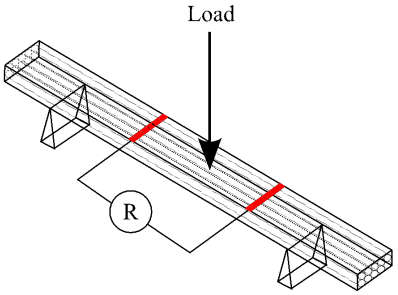

c)

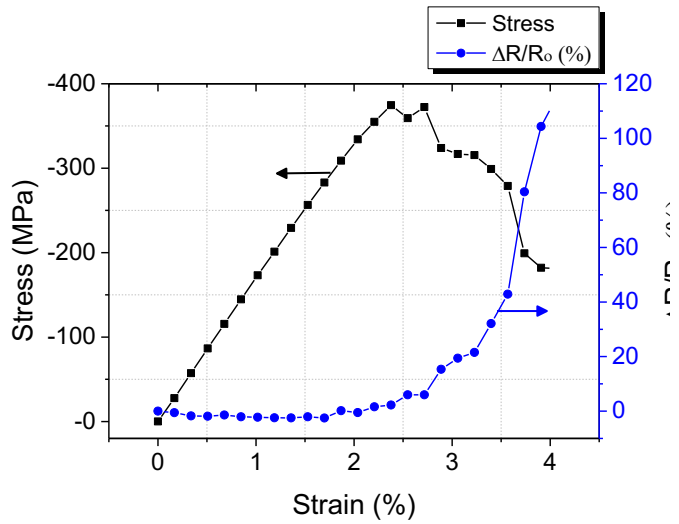

d)

Figure 16.

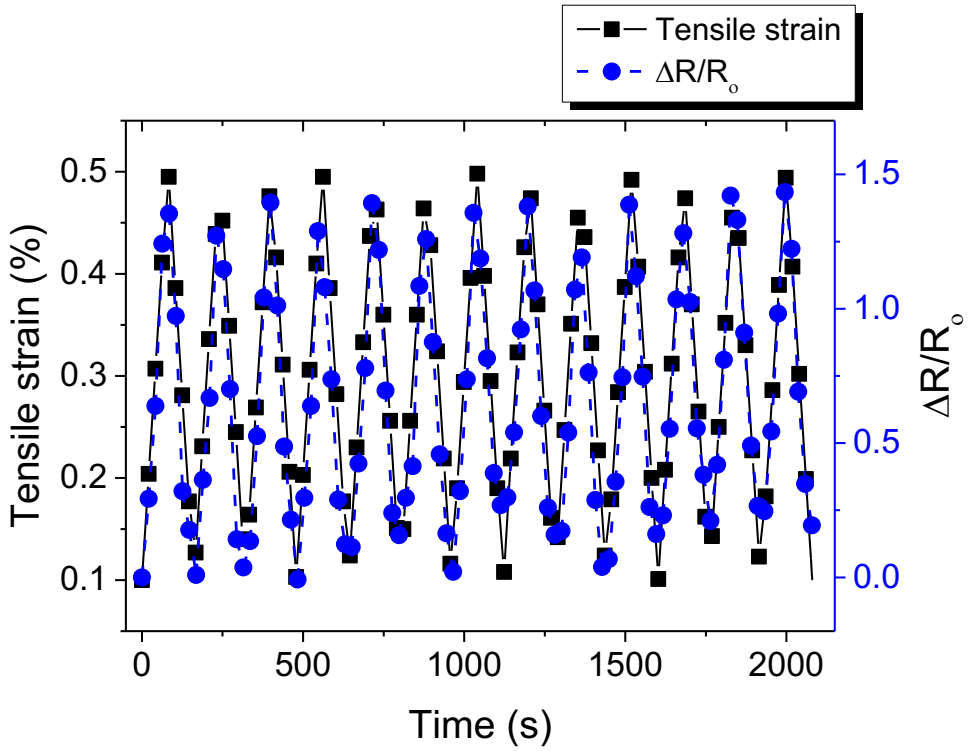

Figure 17.

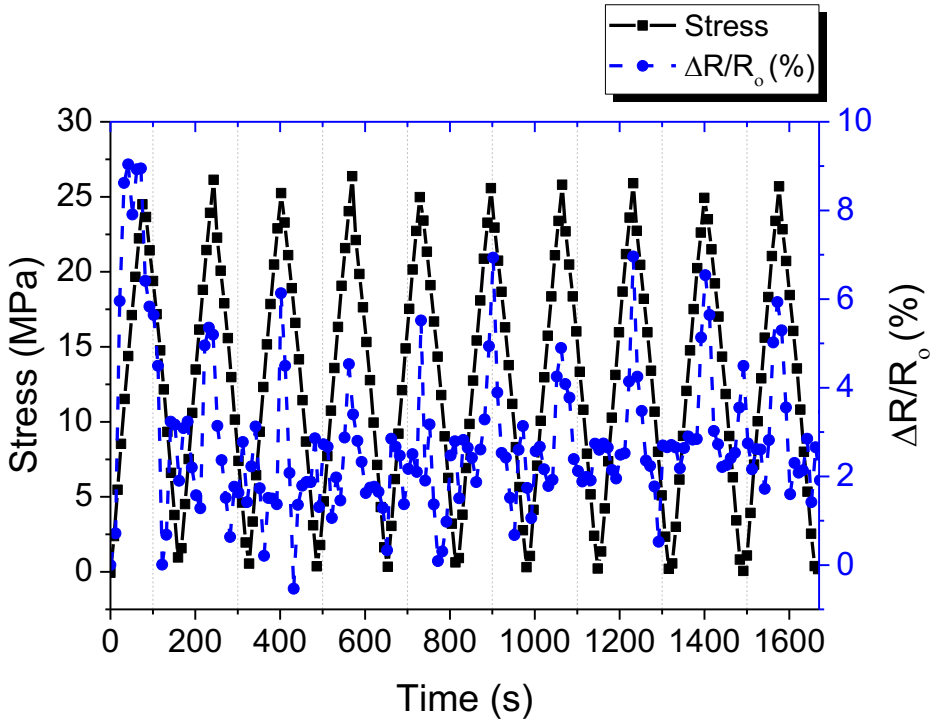

Table 1. Physical properties of epoxy resin.

Physical Property	Value
Glass transition temperature (T_g)	33 °C
Thermal degradation	340 °C
Tensile strength (σ_y) (MPa)	26.47 ± 4.21
Stress at break (σ_b) (MPa)	19.77 ± 2.26
Strain at break (ε_b) (mm/mm)	0.17 ± 0.04

Table 2. Mechanical properties of glass fiber as determined from single fiber tensile tests.

Parameter	Meaning	Value
N	number of specimens	31
$\overline{R}$	average strength at L = 20mm	2402 MPa
σ_0	scale parameter of the Weibull distribution	3551 MPa
m	shape parameter of the Weibull distribution	4.4
υ	coefficient of variation	26.3 %

Table 3. Elemental analysis of GO and rGO specimens as obtained from XPS analysis.

Sample	O (%)	C (%)
GO	34.2	65.8
rGO	9.9	90.1

Table 4. Comparison of ISS values according to Kelly–Tyson model as determined by average fragment length and tensile strength of fiber for uncoated [23], GO coated [23] and rGO coated fibers composites.

Fiber condition	Average fragment length, L_s (mm)	Critical length, L_c (mm)	Fiber strength at the critical length, $\sigma_{fb}(L_c)$ (MPa)	Interlaminar shear strength, ISS (MPa)
Uncoated	2.7 ± 0.9	3.5 ± 1.2	3548.2 ± 267.5	9.0 ± 3.5 [23]
GO coated	0.9 ± 0.1	1.3 ± 0.1	4436.0 ± 111.9	28.6 ± 3.9 [23]
rGO coated	1.6 ± 0.3	2.1 ± 0.4	3940.9 ± 167.9	15.2 ± 3.7

Table 5. Mode I fracture toughness (G_{Ic}) values of Ep-GF, Ep-GO-GF and Ep-rGO-GF composites.

Specimen	Nonlinearity (NL)	Visual observation (VIS)	Maximum load (MAX)
	(J/m^2)	*(J/m^2)*	*(J/m^2)*
Ep-GF	243.5 ± 21.5	401.8 ± 46.3	1176.4 ± 244.9
Ep-GO-GF	384.3 ± 92.6	692.9 ± 145.1	1275.8 ± 180.5
Ep-rGO-GF	352.8 ± 27.0	407.9 ± 52.8	1153.2 ± 141.7

Table 6.

Fiber type with coating	Coating/Deposition process	Mechanical improvement	Interphase bonding phenomenon	Reference
Current work	EPD	IFSS = Improvement of ~217% for GO, Improvement of ~70% for rGO; ILSS = 15% improvement for GO and improvement of 9% for rGO; Flexural properties = ~20% improvement in modulus and strength for GO	Covalent bonding + mechanical interlocking	
Carbon fiber (CF) coated by silanized GO	Dipping	IFSS = 60% improvement; ILSS = 19% improvement; Flexural strength, modulus by 15%	Van der Waals + chemical bonding	[37]
GF coated by GO	Grafting via covalent immobilization	ILSS = 41% improvement	Mechanical locking + covalent bonding	[22]
CF coated with GnP	Solution coating process	Flexural strength increase by 82%; ILSS improvement by 19%	Failure mode: hybrid interfacial/cohesive +	[38]

			mechanical interlocking	
CF (sized) coated with functionalized GO	Grafting	ILSS = 53% improvement	chemical bonding at the interface	[39]
CF coated with GO	Tandem oxidation-ultrasonically assisted EPD	ILSS = 56% improvement	Hydrogen bonding at the interface	[40]
CF coated with GO	epoxy/GO sizing	IFSS = 70.9% improvement; ILSS = 12.7% improvement	chemical bonding at the interface	[41]

Table 7. Creep compliance components and their fitting parameters of the composites Ep-GF, Ep-GO-GF and Ep-rGO-GF (T = 30°C, σ = 5 MPa).

	Creep compliance parameters			**Fitting parameters (Findley's model)**			
	D_e (GPa^{-1})	D_{ve2000} (GPa^{-1})	D_{t2000} (GPa^{-1})	D_e (GPa^{-1})	K (GPa^{-1} s^{-n})	n	R^2
Ep-GF	0.094	0.213	0.307	0.064	0.028	0.3	0.99832
Ep-GO-GF	0.035	0.077	0.112	0.025	0.009	0.3	0.99882
Ep-rGO-GF	0.064	0.053	0.117	0.067	0.0008	0.5	0.99745